

Formulation of an extended null channel formalism for a triangular gravitational wave interferometer configuration in the case of non-identical and correlated noise

Kamiel Janssens^{1,2}, Guillaume Boileau¹, Marie-Anne Bizouard²,
Nelson Christensen², Tania Regimbau³, and Nick van Remortel¹

¹*Universiteit Antwerpen, Prinsstraat 13, 2000 Antwerpen, Belgium*

²*Artemis, Université Côte d'Azur, Observatoire Côte d'Azur, Nice, France*

³*Laboratoire d'Annecy de Physique des Particules,
CNRS, 9 Chemin de Bellevue, 74941 Annecy, France*

(Dated: June 27, 2022)

Several proposed gravitational wave interferometers have a triangular configuration, such as the Einstein Telescope and the Laser Interferometer Space Antenna. For such a configuration one can construct a unique null channel insensitive to gravitational waves from all directions. We expand on earlier work and describe an extended null channel formalism applicable to interferometric data with non-identical as well as correlated noise sources between the different interferometers. Two examples are shown to illustrate the formalism in the context of the Einstein Telescope. Finally we highlight future research needed to transition from the mathematical formalism described here to a framework in which the formalism can be used to estimate the noise power spectral densities of the observing gravitational-wave interferometers.

I. INTRODUCTION

The Einstein Telescope (ET) [1] and Cosmic Explorer (CE) [2, 3] are respectively the European and U.S. proposals for third generation Earth-based interferometric gravitational-wave (GW) detectors. They are planned to outperform the current generation of gravitational wave (GW) interferometers, LIGO [4], Virgo [5] and KAGRA [6], by an order of magnitude in strain sensitivity. The current proposal for ET consists of an equilateral triangle built-up with six interferometers (three for low frequency, three for high frequency), with an opening angle of $\pi/3$ and arm lengths of 10 km. In the rest of this paper, we ignore the details of the xylophone configuration and treat ET as three interferometers [7]. The CE is planned to be an L-shaped interferometer with an arm length of 40 km.

The future space-based GW detector Laser Interferometer Space Antenna (LISA) [8], has also an equilateral triangular configuration, however the length of the arms is 2.5×10^6 km. Whereas ET and CE will be sensitive to GWs with frequencies of a couple of Hz to a couple of kHz, LISA is sensitive to GWs with frequencies between 0.01 mHz and 1 Hz.

Typical astrophysical sources of Earth-based GW detectors are compact binary coalescences (CBCs) such as the binary black hole (BBH), binary neutron star (BNS) and neutron star black hole (NSBH) mergers observed by the LIGO, Virgo and KAGRA collaborations [9–14]. Examples of some other astrophysical GW sources that could be observed by Earth-based GW detectors are transients from core collapse supernova explosions, long-duration GWs from non-asymmetrical heavy objects, such as neutron stars, and the stochastic superposition of a large number of (unresolved) GW signals, such as CBC events [15]. The latter is one of the many sources of the stochastic gravitational wave background

(SGWB) [16].

Typical astrophysical sources for LISA are the coalescence of massive black hole binaries, extreme mass ratio inspirals, and the early inspiral phase of stellar mass CBC events as observed by Earth-based GW interferometers. The non-resolved inspiral of double white dwarf binaries in our galaxy will be the galactic foreground [8].

Given the expected sensitivities for ET, CE and LISA, it is predicted they will observe a large number of overlapping signals [8, 17, 18]. The constant presence of numerous signals will make the estimation of the noise power spectral density (PSD) of these interferometers challenging, while unbiased noise PSD estimation is a key ingredient for all GW detection pipelines.

Another issue that one might face when analyzing the data of ET and LISA is the presence of non-negligible amounts of correlated noise between the different interferometers, due to (almost) co-located terminal stations between the different interferometers. Correlated noise is particularly problematic for unmodeled sources for GWs which depend on cross correlation methods, i.e. searches for poorly known transient signals – called ‘bursts’ – such as the core collapse supernova and the search for a SGWB. The issue of correlated noise on the search for a SGWB using co-located interferometers is well demonstrated by the analysis of the data of the two co-located LIGO Hanford interferometers H1 and H2 taken during the fifth science run (S5). Despite much work on understanding and removing effects from correlated noise, large portions of the data, including all frequencies below 460 Hz, could not be used due to non-negligible effects of correlated noise [19, 20].

A first method to tackle the challenge of noise PSD estimation is to use joint Bayesian parameter estimation to model the noise PSD and signals simultaneously [21, 22]. However more work is needed, to demonstrate how it should work in the presence of many signals, as well as

non-identical and correlated noise.

A second method relies on the sky location independent null channel¹ which is insensitive to GWs. General relativity predicts GWs from two tensor polarisations, the so called 'plus' and 'cross' polarisations. For a network consisting of N detectors one can construct $N - 2$ sky location dependent null streams [23–27]. However, in the case of a triangular configuration of three interferometers, there is one unique null channel which is insensitive to GWs from every direction [17, 28, 29]. Due to imperfect knowledge on the sky location of the source it is difficult to use the sky location dependent null channel for noise PSD estimation. For future detectors such as ET, CE and LISA, it is even practically impossible due to the high probability of overlapping signals. As soon as there are overlapping signals present in the detector the sky location dependent null channel is unable to remove the multiple signals simultaneously due to their different sky locations.

In this paper we focus on the sky location independent null channel which can be constructed for triangular interferometer configurations, introduced in Sec. II. In Sec. III we construct a formalism to account for non-identical and correlated noise sources. The sky location independent null channel is only one element of this more general formalism. Afterwards we illustrate the formalism using simulated data for ET in Sec. IV. In Sec. V we describe further work that is needed to use the described formalism for PSD estimation. Here we note that the sky location independent null channel has been demonstrated to give a PSD estimate in the case of ET [17] in the highly idealized scenario with no correlated noise, as well as identical noise for the three different interferometers. A more recent study has investigated the effectiveness of the null channel in the presence of noise transients, also known as glitches [30]. In the context of LISA, correlated noise was considered but the noise contributions were identical to the three different interferometers [31–35]. However in [36], the authors investigate the impact of non-identical noise on the parameter estimation. Finally, we conclude our work in Sec. VI.

In the remainder of the paper we will refer to the sky location independent null channel as 'unique null channel' or simply 'null channel'.

II. THE NULL CHANNEL

The unique null channel is the sum of the three interferometers in an equilateral triangle, which we will call X , Y and Z . Each detector measures a strain time series $s^I(t)$, which consists both of noise $n^I(t)$ as well as a GW component $h^I(t)$,

$$s^I(t) \equiv n^I(t) + h^I(t), \quad (1)$$

where I runs over X , Y and Z . The null channel is given by the sum of the output of the three interferometers [17]:

$$\begin{aligned} s_{null}(t) &\equiv \sum_{I=X}^Z s^I(t) \\ &= \sum_{I=X}^Z n^I(t) + \sum_{I=X}^Z h^I(t) \\ &= \sum_{I=X}^Z n^I(t) \end{aligned} \quad (2)$$

The derivation of $\sum_{I=X}^Z h^I(t) = 0$ for three interferometers in an equilateral triangle configuration is discussed in earlier work [17]. The equality holds for any polarisation of GW since the sum of the detector response functions of the interferometers is zero. However the calculation assumes the arms of the different interferometers are on top of each other. For the ET, deviations can be expected since the terminal and central stations of two different ET interferometers are separated by about 300m-500m [37]. In this paper we do not consider any of such deviations and assume the interferometers to be exactly on top of each other, leading to a perfect null channel. Furthermore the null channel is not perfect for higher frequencies in an interferometric gravitational-wave detector. This is due to finite arm length effects. There are further imperfections when the arm lengths are not exactly equal, as will be the case for LISA [31]

We introduce the PSD of the strain of interferometer I , S_s^I ,

$$\begin{aligned} \langle s^I(f) s^{I,*}(f') \rangle &= \frac{1}{2} \delta(f - f') S_s^I(f) \\ &= \frac{1}{2} \delta(f - f') [S_n^I(f) + S_h^I(f)], \end{aligned} \quad (3)$$

where $S_n^I(f)$ and $S_h^I(f)$ are respectively the noise and GW PSDs for interferometer I . The cross spectral density (CSD) of the strain of interferometer I and J $S_s^{IJ}(f)$ is given by

$$\begin{aligned} \langle s^I(f) s^{J,*}(f') \rangle &= \frac{1}{2} \delta(f - f') S_s^{IJ}(f) \\ &= \frac{1}{2} \delta(f - f') [S_n^{IJ}(f) + S_h^{IJ}(f)], \end{aligned} \quad (4)$$

where $S_n^{IJ}(f)$ and $S_h^{IJ}(f)$ are respectively the noise and GW CSDs for interferometers I and J .

The quantities $S_h^I(f)$ and $S_h^{IJ}(f)$ depend on the response of the interferometer(s) I and respectively I and J , whereas one typically is interested in $S_h(f)$ of the source regardless of the observing interferometer. The GW signal this paper focuses on is an isotropic SGWB with equal levels of tensor cross- and plus- polarization. However, the formalism we formulate in Sec. III can also be used to estimate noise PSDs for any other GW signal.

¹ The null channel is also known as the null stream or Sagnac channel.

In Appendix A the following equality's are derived for an isotropic SGWB with equal levels of tensor cross- and plus- polarization,

$$\begin{aligned} S_h^I(f) &= \frac{3}{10} S_h(f) \\ S_h^{IJ}(f) &= -\frac{3}{20} S_h(f). \end{aligned} \quad (5)$$

One can already use the null channel for getting information on the detector noise, but even more information can be extracted using a set of three channels A , E and T . These three channels are often used in the context of LISA and are defined as the following linear combinations of the three X , Y and Z interferometers [28, 29]:

$$\begin{aligned} A &= \frac{1}{\sqrt{2}}(Z - X) \\ E &= \frac{1}{\sqrt{6}}(X - 2Y + Z) \\ T &= \frac{1}{\sqrt{3}}(X + Y + Z). \end{aligned} \quad (6)$$

The T channel is a normalized version of the null channel as first defined in Eq. 2 and is insensitive to GWs,

whereas the A and E channels contain the GW signal [29]. Under the assumption of identical noise sources in X , Y and Z , the A , E and T channels are orthogonal with respect to one another, implying that their noise PSDs are uncorrelated.

III. NULL CHANNEL IN A COMPLEX ENVIRONMENT

In this section, we introduce a formalism to expand on the null channel by using the A , E and T channels. First, we discuss the formalism in the presence of identical correlated noise, which already has been studied in the context of LISA [38]. Afterwards, we relax this assumption and describe the most general formalism describing non-identical and correlated noise sources.

A. Formalism in the presence of identical correlated noise

In the presence of correlated noise, identical in all interferometers – $S_n^{XY}(f) = S_n^{XZ}(f) = S_n^{YZ}(f) \equiv S_n^{IJ}(f)$ – as well as assuming identical noise PSDs – $S_n^X(f) = S_n^Y(f) = S_n^Z(f) \equiv S_n^I(f)$ – the following equality's hold for the A , E and T channels

$$\begin{aligned} \langle T(f)T^*(f') \rangle &= \frac{1}{2} \delta(f - f') [S_n^I(f) + 2S_n^{IJ}(f)] \\ \langle A(f)A^*(f') \rangle &= \frac{1}{2} \delta(f - f') \left[S_n^I(f) - S_n^{IJ}(f) + \frac{9}{20} S_h(f) \right] \\ \langle E(f)E^*(f') \rangle &= \frac{1}{2} \delta(f - f') \left[S_n^I(f) - S_n^{IJ}(f) + \frac{9}{20} S_h(f) \right] \\ \langle T(f)A^*(f') \rangle &= \langle A(f)T^*(f') \rangle = 0 \\ \langle T(f)E^*(f') \rangle &= \langle E(f)T^*(f') \rangle = 0 \\ \langle E(f)A^*(f') \rangle &= \langle A(f)E^*(f') \rangle = 0. \end{aligned} \quad (7)$$

Here we assumed the GW signal to be an isotropic SGWB with equal levels of plus- and cross- polarization, for which the contributions to the A and E channels is derived in Appendix A. In Appendix B we also derive the equivalent terms in case of the presence of an isotropic SGWB with scalar or vector polarizations, which are predicted by several extensions of general relativity [39]. However, the normalized null channel, i.e. the T channel, can be used for noise PSD estimation regardless of the GW signal.

We note there is no correlation between any of the A , E and T channels, in line with the expectations since the

channels were constructed as such in the context of LISA [28, 29]. We want to stress that in the case of a fully isotropic SGWB $\langle E(f)A^*(f') \rangle$ is insensitive to the GWs. This result breaks down for different GW sources.

B. Formalism in the presence of non-identical and correlated noise

In the more general scenario where the correlated noise as well as the noise PSDs are unique for each interferometer, the set of equations is given by,

$$\begin{aligned}
\langle T(f)T^*(f') \rangle &= \frac{1}{2}\delta(f-f') \left[\frac{1}{3}(S_n^X(f) + S_n^Y(f) + S_n^Z(f)) + \frac{2}{3}(S_n^{XY}(f) + S_n^{XZ}(f) + S_n^{YZ}(f)) \right] \\
\langle T(f)X^*(f') \rangle = \langle X(f)T^*(f') \rangle &= \frac{1}{2}\delta(f-f') \left[\frac{1}{\sqrt{3}}(S_n^X(f) + S_n^{XY}(f) + S_n^{XZ}(f)) \right] \\
\langle T(f)Y^*(f') \rangle = \langle Y(f)T^*(f') \rangle &= \frac{1}{2}\delta(f-f') \left[\frac{1}{\sqrt{3}}(S_n^Y(f) + S_n^{YX}(f) + S_n^{YZ}(f)) \right] \\
\langle T(f)Z^*(f') \rangle = \langle Z(f)T^*(f') \rangle &= \frac{1}{2}\delta(f-f') \left[\frac{1}{\sqrt{3}}(S_n^Z(f) + S_n^{ZX}(f) + S_n^{ZY}(f)) \right] \\
\langle A(f)A^*(f') \rangle &= \frac{1}{2}\delta(f-f') \left[\frac{1}{2}(S_n^X(f) + S_n^Z(f)) - S_n^{XZ}(f) + \frac{9}{20}S_h(f) \right] \\
\langle E(f)E^*(f') \rangle &= \frac{1}{2}\delta(f-f') \left[\frac{1}{6}(S_n^X(f) + 4S_n^Y(f) + S_n^Z(f)) + \frac{1}{3}S_n^{XZ}(f) - \frac{2}{3}(S_n^{XY}(f) + S_n^{YZ}(f)) \right. \\
&\quad \left. + \frac{9}{20}S_h(f) \right] \\
\langle T(f)A^*(f') \rangle = \langle A(f)T^*(f') \rangle &= \frac{1}{2}\delta(f-f') \left[\frac{1}{\sqrt{6}}(S_n^Z(f) - S_n^X(f) + S_n^{YZ}(f) - S_n^{XY}(f)) \right] \\
\langle T(f)E^*(f') \rangle = \langle E(f)T^*(f') \rangle &= \frac{1}{2}\delta(f-f') \left[\frac{1}{3\sqrt{2}}(S_n^X(f) - 2S_n^Y(f) + S_n^Z(f) - S_n^{XY}(f) + 2S_n^{XZ}(f) - S_n^{YZ}(f)) \right] \\
\langle E(f)A^*(f') \rangle = \langle A(f)E^*(f') \rangle &= \frac{1}{2}\delta(f-f') \left[\frac{1}{2\sqrt{3}}(-S_n^X(f) + S_n^Z(f) - 2S_n^{YZ}(f) + 2S_n^{XY}(f)) \right],
\end{aligned} \tag{8}$$

where as in Eq. 7 the GW signal is assumed to be an isotropic SGWB. Eq. 8 shows the added advantage of using the A , E , T channels over using only the T -channel, namely the cross correlation terms $\langle T(f)A^*(f') \rangle$ and $\langle T(f)E^*(f') \rangle$ contain additional information. They are a measure of the non-identical noise sources present in the X , Y and Z interferometers. We also add the cross correlation terms between the null channel T and the X , Y and Z channels. Their sum is proportional to the PSD of the T channel, but in the case of non-identical noise one can gain by rather using the three correlation channels $\langle T(f)X^*(f') \rangle$, $\langle T(f)Y^*(f') \rangle$ and $\langle T(f)Z^*(f') \rangle$ because this helps disentangling the different noise contributions. However, Eq. 8 also uncovers the great amount of complexity that is present in the most general scenario, where noise and correlated noise are different in the three interferometers.

The formalism described above is summarized in a diagram in Fig 1. In Sec. IV we illustrate the formalism using two examples, whereas in Sec. V we outline the next steps needed to use this formalism in a Bayesian estimation framework.

A method that could be used for transient searches to estimate the false alarm rate in the cross-correlation space could rely on correlating the null channel $T(t)$ with a time-shifted [40] version $T(t + \delta t)$. This ensures the background estimation is free from any contamination from the large amount of transient events. A more detailed study on the utility of this method will be presented in a subsequent paper. For the goal presented in this paper, i.e. estimating the power and cross spectral

densities, time-sliding either the X , Y and Z or the A , E and T channels and correlating these with the non-time shifted null channel does not give any additional information on the quantities $S_n^X(f)$, $S_n^Y(f)$, $S_n^Z(f)$, $S_n^{XY}(f)$, $S_n^{XZ}(f)$ and $S_n^{YZ}(f)$.

IV. EXAMPLES IN THE CONTEXT OF THE EINSTEIN TELESCOPE

In this section, we illustrate the formalism described in Eq. 7 and Eq. 8 using two examples. First, we show that the T channel is insensitive to GWs by injecting an astrophysically produced SGWB coming from CBC events. Secondly, we build a simple toy-model with non-identical as well as correlated noise sources to demonstrate the formalism described in Eq. 8. In this example, the formalism is illustrated in the context of the ET; however, one could use to formula's derived in Eq. 7 and Eq. 8 for any equilateral triangular configuration of GW interferometers.

In future work one should build on this formalism to develop a Bayesian inference model which enables the user to estimate the different (un)correlated noise sources using the formalism summarized in Fig. 1 and which will be further discussed in Sec. V.

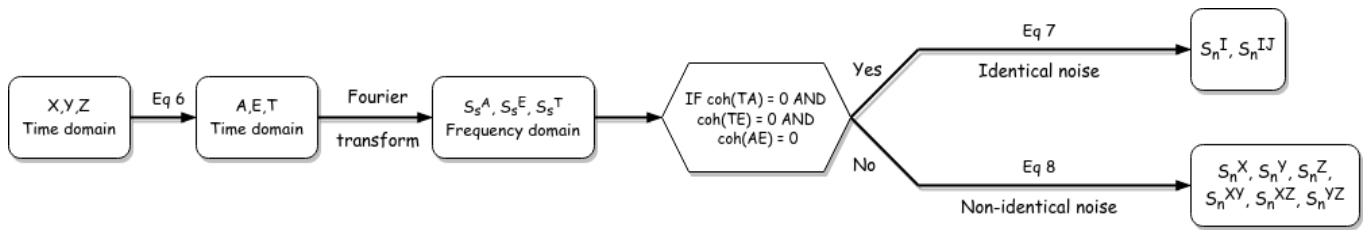


FIG. 1: Diagram summarizing the formalism one can use for the estimation of noise spectral densities. In the presence of non-identical noise more information can be gained by using the CSD between TX , TY and TZ compared to just using the PSD TT , as shown in Eq. 8

A. The null channel in the presence of GWs

For this demonstration, we use 2048 seconds of data with an artificially enhanced SGWB coming from CBC events, injected on top of Gaussian noise colored with the design sensitivity of the xylophone configuration of the ET². In the rest of the paper we will refer to this colored Gaussian noise as 'ET noise' and introduce the following notation for this noise S_n^{ET} . Note that despite the fact that we use identical noise, the X , Y and Z data are different Gaussian noise realisations.

The SGWB coming from CBC events is expected to be (one of) the first GW background signal(s) that will be observed by ground-based interferometers [41]. One typically wants to measure the normalized energy density of the SGWB, expressed by [42, 43]

$$\Omega_{\text{GW}}(f) = \frac{1}{\rho_c} \frac{d\rho_{\text{GW}}}{d \ln f}, \quad (9)$$

where $d\rho_{\text{GW}}$, is the energy density contained in a logarithmic frequency interval, $d \ln f$. Here, $\rho_c = 3H_0^2 c^2 / (8\pi G)$ is the critical energy density for a flat Universe. In the absence of correlated noise one can construct a cross-correlation statistic which is an unbiased estimator of $\Omega_{\text{GW}}(f)$ as follows,

$$\hat{C}_{IJ}(f) = \frac{2}{\Delta T} \frac{\text{Re}[\tilde{s}_I^*(f)\tilde{s}_J(f)]}{\gamma_{IJ}(f)S_0(f)}, \quad (10)$$

for interferometers I and J , where $\tilde{s}_I(f)$ is the Fourier transform of the time domain strain data $s_I(t)$ measured by interferometer I , and γ_{IJ} the normalized overlap reduction function which encodes the baseline's geometry [43, 44]. $S_0(f)$ is a normalization factor given by $S_0(f) = (9H_0^2)/(40\pi^2 f^3)$ and ΔT is the time duration of the data used.

The energy density $\Omega_{\text{GW}}(f)$ of the SGWB coming from unresolved CBC events is predicted to behave as a power law, with a slope of $\alpha = 2/3$, at lower frequencies where all the sources contribute in their inspiral phase [45, 46].

We assume the GW signal consists of equal parts tensorial plus- and cross-polarization, as expected by general relativity. Given the normalization constant $S_0(f)$ contains a factor f^{-3} , this implies $\text{Re}[\tilde{s}_I^*(f)\tilde{s}_J(f)] \propto f^{-7/3}$.

The left panel of Fig. 2 shows the PSDs for the X , Y and Z channels in the presence of this SGWB and compares with the ET noise S_n^{ET} . In this scenario, the SGWB is dominant over the ET noise up to 30 Hz and is, as expected, proportional to $\propto f^{-7/3}$. The right panel of Fig. 2 shows the PSDs for the A , E and T channels for the same data. Foremost, we notice that, as expected, the T channel – which is a normalized null channel – is insensitive to the GW signals. From Eq. 7 one would expect the A and E channels to be identical, which is only true to a good approximation as one can see from the right panel of Fig. 2. A first possible reason are the different Gaussian noise realisations in the X , Y and Z , channels, however this is expected to be a small effect. The dominant effect is coming from unequal GW contributions in the X , Y and Z interferometers. The GW signal in the different channels has an average amplitude difference of about 3.5% to 7% in the 5Hz to 300Hz frequency band. This difference is likely due to the short duration of analysed data (2048 seconds), which contains 1071 CBC events in our simulated data. The limited amount of events does not allow for a fully isotropic distribution, leading to the observed difference. Given the different contributions of the X , Y and Z channels relative to the A and E channels, their respective GW components differ by an average amplitude difference of $\approx 4\%$ compared to the signal we expect from Eq. 7 and the contribution derived in Appendix A. The expected signal for the A and E channels is also shown in the right panel of Fig. 2, where we have approximated S_n^{ET} by the average of S_n^I and S_n^h by the average of S_n^I , with $I = X, Y, Z$. Please note that for estimating S_n^h a factor of 10/3 appears to describe its relation to S_n^I as indicated by Eq. 5.

B. Non-identical and correlated noise

We now implement a toy-model with correlated noise between different interferometer pairs. The X , Y and Z channels all share the same ET noise S_n^{ET} . In addition to this we inject, in the time-domain, Gaussian

² This design is often also referred to as ET-D.

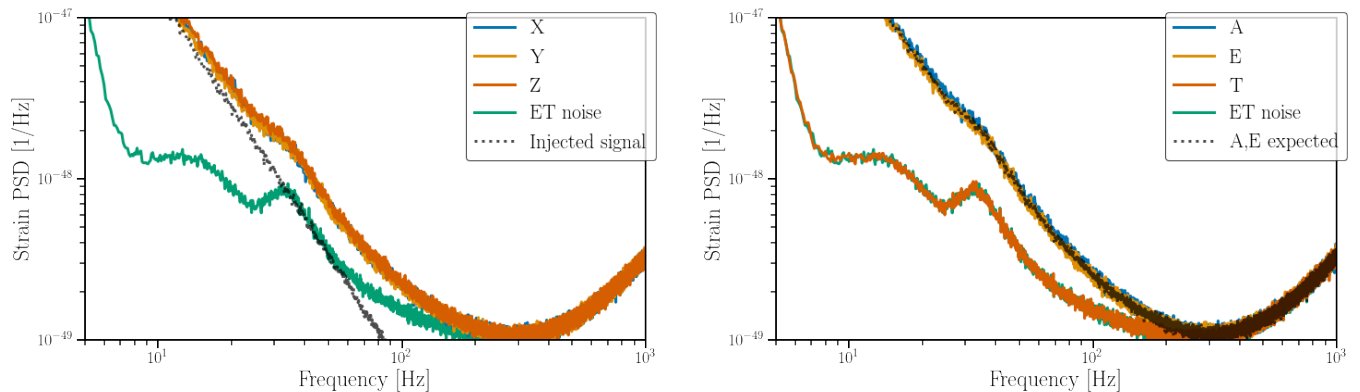


FIG. 2: Left: the PSDs of the X , Y , Z channels and the ET noise and of the injected SGWB coming from CBC events. Right: the power spectral densities of the associated A , E and T channels and the ET noise. Furthermore, we show the expected PSD associated to the A and E channels as calculated by the formalism (Eq. 7 and 8), see the text for more information. The T channel – a normalized version of the null channel - is insensitive to GWs.

peaks with a standard deviation of 1Hz and means of 10 Hz, 50 Hz and 90 Hz. The strain peak amplitude of the Gaussian peaks at 10Hz and 50Hz is $\sim 1.1 \times 10^{-24} \frac{1}{\sqrt{\text{Hz}}}$, whereas the amplitude of the Gaussian peak at 90Hz is $\sim 5.7 \times 10^{-25} \frac{1}{\sqrt{\text{Hz}}}$. In every interferometer, we inject two of these Gaussian peaks such that the X , Y and Z channels have one correlated Gaussian peak with respect to the two other interferometers. We coherently inject Gaussian peaks at 10Hz and 50Hz in the X interferometer, at 10 Hz and 90 Hz in the Y interferometer and at 50 Hz and 90 Hz in the Z interferometer. The PSDs of the X , Y and Z interferometers are shown in the left panel of Fig. 3, using 2048 seconds of data. The Gaussian peaks are clearly visible in the data set. The right panel of Fig. 3 shows the A , E and T channels. First, we notice the three Gaussian peaks appear with different contributions in the A , E and T channels. Important to note here is that the T channel is sensitive to correlated noise, as shown in Eq. 7 and Eq. 8, since only GW signals cancel each other due to the specific way in which they couple to our interferometers, that is through the detector response functions.

In the right panel of Fig. 3 we show the A , E and T channels subtracted from the contributions of the Gaussian peaks for which we define their PSDs as $S_n^{\text{GP}10}$, $S_n^{\text{GP}50}$ and $S_n^{\text{GP}90}$ for respectively the Gaussian peaks with a mean of 10 Hz, 50 Hz and 90 Hz. The following equality holds for the X channel, $S_n^X = S_n^{\text{ET},X} + S_n^{\text{GP}10} + S_n^{\text{GP}50}$, where $S_n^{\text{ET},X}$ has a different Gaussian noise realisation than $S_n^{\text{ET},Y}$ and $S_n^{\text{ET},Z}$. Using this equality, as well as the respective equalities for the Y and Z channels we subtract the PSD from the Gaussian peaks in the frequency domain as calculated by their contributions in Eq. 8 such that the expected residual is S_n^{ET} , that is the ET noise. For this demonstration we assume we know the PSD of the Gaussian peaks. As can be seen in the right panel of Fig. 3, the subtracted A , E and T channels agree well with the ET noise. However, we note that

near the center of the Gaussian peak after subtraction, the variance has increased.

As mentioned in Sec. III, the cross correlation between the T and A , E channels ($S_s^{TA}(f)$ and $S_s^{TE}(f)$) contains additional information on the non-identical character of the correlated noise. The left panel of Fig. 4 shows the coherence between the T channel and the A and E channels. This coherence is consistent with coming from Gaussian noise³ apart from the Gaussian peaks. This indicates, correctly, that the only part of the noise in the X , Y and Z channels which isn't identical are the Gaussian peaks. The right panel of Fig. 4 shows the accompanying cross spectral density. We also show the expected contribution from $S_s^{TA}(f)$ and $S_s^{TE}(f)$ where the contributions of the Gaussian peaks ($S_n^{\text{GP}10}$, $S_n^{\text{GP}50}$ and $S_n^{\text{GP}90}$) are subtracted as calculated by their contributions in Eq. 8. The result is consistent with the cross-spectral density of two different Gaussian instantiations of the ET noise.

Fig. 5 compares the cross spectral density $S_s^{TX}(f)$ with the power spectral density $S_s^T(f)$. Please note that we have multiplied $S_s^{TX}(f)$ with a factor of $\sqrt{3}$ as given by Eq. 8 such that the spectral density equals the ET noise apart from the Gaussian peaks which are additionally injected in the data. We also show that when the contribution from the Gaussian noise peaks is subtracted as calculated in Eq. 8, the data is consistent with the ET noise. The amplitude of the Gaussian peaks at 10Hz and 50Hz are slightly different in $S_s^{TX}(f)$, compared to $S_s^T(f)$. This is expected and follows from the different proportions of the peaks in the X and T channels. Equivalent to $S_s^{TX}(f)$ one can also construct $S_s^{TY}(f)$ and $S_s^{TZ}(f)$, which are equivalent with the only difference being the location of the two peaks. Using $S_s^{TX}(f)$, $S_s^{TX}(f)$

³ The expected coherence for uncorrelated data goes approximately as $1/N$, where N is the number of time segments over which the coherence is averaged.

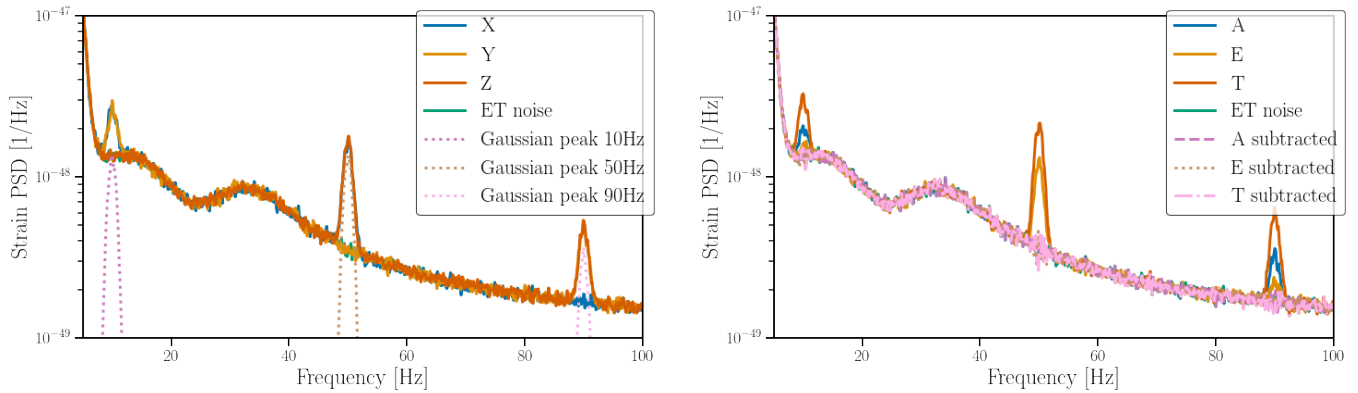


FIG. 3: Left: the PSDs of the X , Y , Z channels, the ET noise and the injected correlated noise (see text for a more detailed description). Right: the PSDs of the associated A , E and T channels and the ET noise. Furthermore, the power spectral densities associated with the A , E and T channels are shown where the PSD contribution from the Gaussian peaks is subtracted in the frequency domain as calculated in Eq. 8, see the text for more information. The subtracted data is, as expected, consistent with the ET noise.

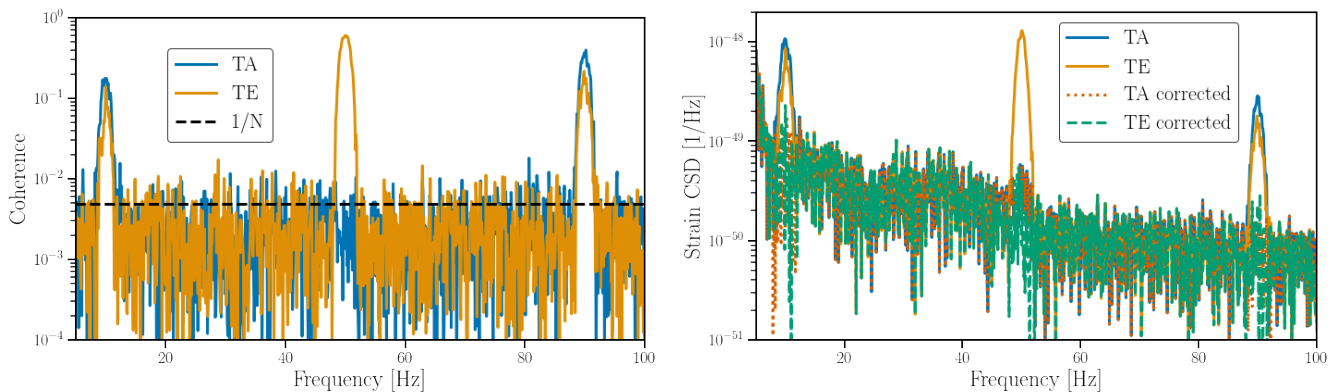


FIG. 4: Left: the coherence between the T and A , E channels. The black dashed line represents the level of coherence expected from independent Gaussian data, which goes approximately as $1/N$, where N is the number of time segments over which was averaged. Right: the cross spectral density between the T and A , E channels.

Furthermore, the cross spectral densities associated with the TA , and TE channels are shown where the contribution from the Gaussian noise peaks is subtracted as calculated in Eq. 8, see the text for more information. The subtracted data is consistent with the cross spectral density between two different Gaussian noise instantiations of the ET noise.

and $S_s^{TZ}(f)$ channels rather than using the PSD of the null channel $S_s^T(f)$, one would be able to make more accurate estimations of the noise spectral densities S_n^X , S_n^Y , S_n^Z , S_n^{XY} , S_n^{XZ} and S_n^{YZ} since the three separate cross correlations contain more information regarding the non-identical behaviour and the proportions in the different X , Y and Z channels.

V. RECIPE TO TRANSFORM THE EXTENDED NULL CHANNEL FORMALISM INTO A PSD ESTIMATION FRAMEWORK

In previous sections, we have shown how one can construct the sky location independent null channel for an

equilateral triangular GW interferometer configuration in a situation where there is correlated noise unique to each detector pair, as well as where all the interferometers might have different noise levels. However, this examples assumed toy noise models as well as perfect knowledge of these noise sources. In a real scenario for the ET, both these assumptions will break down. In this section, we propose further investigations so that one can estimate the noise PSDs as well as correlated noise levels for ET (or LISA) to observe GWs.

After the proof of concept of the A , E and T channels for the ET in earlier sections, one should develop a Bayesian framework to enable parameter estimation of the noise PSDs as well as correlated noise PSDs, that is S_n^I and S_n^{IJ} or in the more general scenario S_n^X , S_n^Y , S_n^Z ,

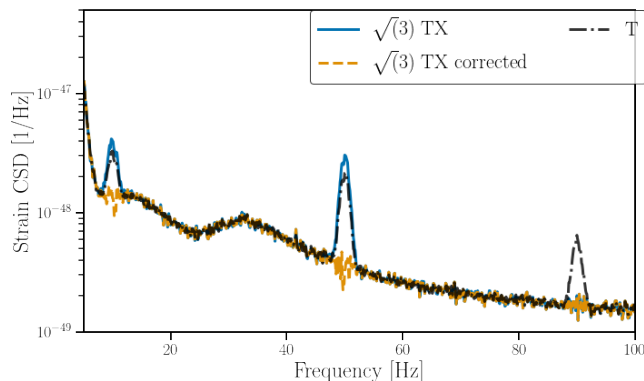


FIG. 5: The cross spectral density between the T and X channel is compared to the power spectral density of the T channel. Furthermore, the cross spectral densities associated with the TX , is shown where the contribution from the Gaussian noise peaks is subtracted as calculated in Eq. 8, see the text for more information. The subtracted data is consistent with the ET noise as we have multiplied the CSD of the TX channels with a factor of $\sqrt{3}$.

S_n^{XY} , S_n^{XZ} and S_n^{YZ} [21, 22]. Here one should consider multiple scenarios such as identical noise sources, unique noise sources for each X , Y and Z interferometer, absence/presence of correlated noise. In the case of non-identical noise sources for the different interferometers it is beneficial to use the cross-correlation of the null channel T with the X , Y and Z channels ($S_s^{TX}(f)$, $S_s^{TY}(f)$ and $S_s^{TZ}(f)$) rather than using the PSD of T ($S_s^T(f)$) to estimate the noise sources in the different interferometers. More information on the non-identical noise components in the X , Y and Z channels is contained in the cross spectral density of the null channel with the A and E channels ($S_s^{TA}(f)$ and $S_s^{TE}(f)$). Furthermore, one should understand the effect of knowledge on (un)correlated noise sources, from possible witness sensors observing the noise sources (e.g. magnetometers, seismometers, etc.), and how this can improve the final parameter estimation of the noise PSDs. Given the high dimensional problem, estimations of all the parameters with the desired accuracy might prove difficult in the most general scenario and more work is needed to achieve such a goal. To this extent, one should also take the non-stationary character of real data into account. This implies it is not trivial to just extend the duration of the data used to compute the different noise contributions using the extended null channel formalism, presented in this paper.

Third and finally, the knowledge on correlated noise sources and their properties should be understood and studied further if one wants to simulate a realistic scenario for the above techniques. In the context of the search for a SGWB using Earth-based interferometers there have already been significant investigations concerning the effects of correlated magnetic fields, e.g.

Schumann resonances [47–53], also in the context of ET [54]. A recent paper studies correlated seismic and Newtonian noise over distances of several hundreds of meters⁴ and their impact on stochastic searches using the ET [55]. These results for the ideal starting point for studying correlated noise in the formalism described in this paper but more dedicated follow-up studies could look into the effect from earthquakes, the possibility of correlated seismic fields on the scale of 10km and the interplay between different coupling locations and to which extent there is constructive or destructive interference between e.g. correlated magnetic fields coupling to both input and end mirrors of the interferometers.

For LISA noise correlation studies resulting from the spatial environment can benefit from more detailed noise characterisation. These noises include for example the effect of micro-thrusters, the magnetic field and the temperature variations on the test-mass system [56].

These research topics pose fundamental questions for understanding the data analysis environment at ET, and should be studied in significantly more detail over the course of the coming years before the ET becomes operational to ensure the ET can fulfill its scientific goals. This is especially true for correlated noise, which would seriously affect the search for a SGWB.

VI. CONCLUSION

Future GW interferometers such as ET, CE and LISA will have sensitivities allowing them to resolve many transient sources to such an extent that they are expected to observe a large amount of overlapping signals [8, 17, 18]. This makes it difficult to estimate the noise PSD of the interferometers needed to perform GW searches.

A first method is to simultaneously model noise and signals using for instance a joint Bayesian parameter estimation framework [21, 22]. This paper is investigating a different approach relying on the sky location independent null channel which can be constructed for triangular configurations of interferometers ET and LISA. This sky location independent null channel is insensitive to GWs from any direction.

We introduce a formalism which is able to not only address correlated noise between the different interferometers, but also allow for non-identical noise both correlated and uncorrelated. The formalism goes beyond using the sky location independent null channel and relies on three linear combinations A , E and T of the three interferometers X , Y and Z , which have been used in LISA before [28, 29]. The advantage of relying on the A , E and T channels, of which the T channel is a normalized version of the null channel, is that their cross-correlation

⁴ 300m-500m is the expected distance between the terminal and central stations of two different ET interferometers [37].

spectra contain additional information in the case of non-identical noise sources. We also explain how correlating the null channel with the X , Y and Z channels will allow more accurate estimation of your noise PSDs and CSDs in the case of non-identical noise compared to just using the null channel.

We illustrate the formalism using two examples for the ET. In the first example an isotropic SGWB coming from CBC events was injected, where we show the T channel is indeed insensitive to gravitational waves. Due to the limited amount of data used in this example the injected events, the injected SGWB isn't fully isotropic, leading to small deviations in the observed A and E signals compared to the calculated values for a fully isotropic SGWB. In the second example we investigate non-identical and correlated noise and show that with knowledge of these correlated noise sources our formalism can be used to subtract these from the A , E and T channels.

Finally in Sec. V we discuss the steps needed to go from the formalism described here to a working Bayesian

estimation framework able to estimate the different non-identical and correlated noise sources for a triangular interferometer configuration.

ACKNOWLEDGMENTS

The authors acknowledge access to computational resources provided by the LIGO Laboratory supported by National Science Foundation Grants PHY-0757058 and PHY-0823459. GB thanks the laboratory Artemis, Observatoire de la Côte d'Azur, for hospitality and welcome.

Furthermore, the authors would like to thank Q. Baghi, B. Goncharov, S. Shah and O. Hartwig for useful comments.

This paper has been given LIGO DCC number P2200126, Virgo TDS number VIR-0443A-22 and ET TDS number ET-0066A-22.

K.J. is supported by FWO-Vlaanderen via grant number 11C5720N.

-
- [1] M. Punturo *et al.*, *Class. Quant. Grav.* **27**, 194002 (2010).
 - [2] D. Reitze, R. X. Adhikari, S. Ballmer, B. Barish, L. Barsotti, G. Billingsley, D. A. Brown, Y. Chen, D. Coyne, R. Eisenstein, M. Evans, P. Fritschel, E. D. Hall, A. Lazzarini, G. Lovelace, J. Read, B. S. Sathyaprakash, D. Shoemaker, J. Smith, C. Torrie, S. Vitale, R. Weiss, C. Wipf, and M. Zucker, *Bulletin of the AAS* **51** (2019), <https://baas.aas.org/pub/2020n7i035>.
 - [3] M. Evans *et al.*, (2021), arXiv:2109.09882 [astro-ph.IM].
 - [4] J. Aasi *et al.* (LIGO Scientific Collaboration), *Classical and Quantum Gravity* **32**, 074001 (2015).
 - [5] F. Acernese *et al.* (Virgo Collaboration), *Class. Quant. Grav.* **32**, 024001 (2015), arXiv:1408.3978 [gr-qc].
 - [6] Y. Aso, Y. Michimura, K. Somiya, M. Ando, O. Miyakawa, T. Sekiguchi, D. Tatsumi, and H. Yamamoto (KAGRA Collaboration), *Phys. Rev. D* **88**, 043007 (2013).
 - [7] S. Hild *et al.*, *Class. Quant. Grav.* **28**, 094013 (2011), arXiv:1012.0908 [gr-qc].
 - [8] P. Amaro-Seoane *et al.*, arXiv e-prints, arXiv:1702.00786 (2017), arXiv:1702.00786 [astro-ph.IM].
 - [9] B. P. Abbott *et al.* (LIGO Scientific Collaboration and Virgo Collaboration), *Phys. Rev. Lett.* **116**, 061102 (2016).
 - [10] B. P. Abbott *et al.* (LIGO Scientific Collaboration and Virgo Collaboration), *Phys. Rev. X* **9**, 031040 (2019).
 - [11] R. Abbott *et al.* (LIGO Scientific Collaboration and Virgo Collaboration), arXiv e-prints, arXiv:2010.14527 (2020), arXiv:2010.14527 [gr-qc].
 - [12] R. Abbott *et al.* (The LIGO Scientific Collaboration and the Virgo Collaboration), “Gwtc-2.1: Deep extended catalog of compact binary coalescences observed by ligo and virgo during the first half of the third observing run,” (2021), arXiv:2108.01045 [gr-qc].
 - [13] R. Abbott *et al.* (LIGO Scientific Collaboration, Virgo Collaboration and KAGRA collaboration), *The Astrophysical Journal Letters* **915**, L5 (2021).
 - [14] R. Abbott *et al.* (The LIGO Scientific Collaboration and the Virgo Collaboration and the KAGRA Collaboration), “Gwtc-3: Compact binary coalescences observed by ligo and virgo during the second part of the third observing run,” (2021), arXiv:2111.03606 [gr-qc].
 - [15] K. Riles, *Progress in Particle and Nuclear Physics* **68**, 1–54 (2013).
 - [16] N. Christensen, *Reports on Progress in Physics* **82**, 016903 (2018).
 - [17] T. Regimbau, T. Dent, W. Del Pozzo, S. Giampanis, T. G. F. Li, C. Robinson, C. Van Den Broeck, D. Meacher, C. Rodriguez, B. S. Sathyaprakash, and K. Wójcik, *Phys. Rev. D* **86**, 122001 (2012).
 - [18] T. Regimbau and S. A. Hughes, *Phys. Rev. D* **79**, 062002 (2009).
 - [19] N. V. Fotopoulos and the LIGO Scientific Collaboration, *Journal of Physics: Conference Series* **122**, 012032 (2008).
 - [20] J. Aasi *et al.* (LIGO Scientific Collaboration and Virgo Collaboration), *Phys. Rev. D* **91**, 022003 (2015).
 - [21] M. C. Edwards, R. Meyer, and N. Christensen, *Phys. Rev. D* **92**, 064011 (2015).
 - [22] N. Christensen and R. Meyer, *Rev. Mod. Phys.* **94**, 025001 (2022), arXiv:2204.04449 [gr-qc].
 - [23] Y. Gürsel and M. Tinto, *Phys. Rev. D* **40**, 3884 (1989).
 - [24] L. Wen and B. F. Schutz, *Classical and Quantum Gravity* **22**, S1321 (2005).
 - [25] L. Wen, X. Fan, and Y. Chen, *Journal of Physics: Conference Series* **122**, 012038 (2008).
 - [26] L. Wen and Y. Chen, *Phys. Rev. D* **81**, 082001 (2010).
 - [27] P. J. Sutton *et al.*, *New J. Phys.* **12**, 053034 (2010), arXiv:0908.3665 [gr-qc].
 - [28] M. Tinto and S. V. Dhurandhar, *Living Reviews in Relativity* **8** (2005), 10.12942/lrr-2005-4.
 - [29] T. L. Smith and R. R. Caldwell, *Phys. Rev. D* **100**, 104055 (2019).
 - [30] B. Goncharov, A. H. Nitz, and J. Harms, “Utilizing the

- null stream of einstein telescope,” (2022).
- [31] M. R. Adams and N. J. Cornish, Phys. Rev. D **82**, 022002 (2010).
- [32] M. R. Adams, “Detecting a stochastic gravitational wave background with space-based interferometers,” (2014), <https://scholarworks.montana.edu/xmlui/handle/1/3607>.
- [33] G. Boileau, N. Christensen, R. Meyer, and N. J. Cornish, Phys. Rev. D **103**, 103529 (2021), arXiv:2011.05055 [gr-qc].
- [34] G. Boileau, A. Lamberts, N. Christensen, N. J. Cornish, and R. Meyer, Monthly Notices of the Royal Astronomical Society **508**, 803 (2021), arXiv:2105.04283 [gr-qc].
- [35] G. Boileau, A. C. Jenkins, M. Sakellariadou, R. Meyer, and N. Christensen, Phys. Rev. D **105**, 023510 (2022), arXiv:2109.06552 [gr-qc].
- [36] Q. Baghi, J. I. Thorpe, J. Slutsky, and J. Baker, Phys. Rev. D **103**, 042006 (2021).
- [37] ET Steering Committee Editorial Team, (2020), ET-0007B-20.
- [38] T. A. Prince, M. Tinto, S. L. Larson, and J. W. Armstrong, Phys. Rev. D **66**, 122002 (2002).
- [39] T. Callister, A. S. Biscoveanu, N. Christensen, M. Isi, A. Matas, O. Minazzoli, T. Regimbau, M. Sakellariadou, J. Tasson, and E. Thrane, Phys. Rev. X **7**, 041058 (2017), arXiv:1704.08373 [gr-qc].
- [40] M. Was, M.-A. Bizouard, V. Brisson, F. Cavalier, M. Davier, P. Hello, N. Leroy, F. Robinet, and M. Vavoulidis, Class. Quant. Grav. **27**, 015005 (2010), arXiv:0906.2120 [gr-qc].
- [41] R. Abbott et al. (LIGO Scientific Collaboration, Virgo Collaboration and KAGRA collaboration), Phys. Rev. D **104**, 022004 (2021), arXiv:2101.12130 [gr-qc].
- [42] B. Allen and J. D. Romano, Phys. Rev. D **59**, 102001 (1999).
- [43] J. D. Romano and N. J. Cornish, Living Rev. Rel. **20**, 2 (2017), arXiv:1608.06889 [gr-qc].
- [44] N. Christensen, Phys. Rev. D **46**, 5250 (1992).
- [45] T. Regimbau, Res. Astron. Astrophys. **11**, 369 (2011), arXiv:1101.2762 [astro-ph.CO].
- [46] T. Regimbau, Symmetry **14** (2022), 10.3390/sym14020270.
- [47] E. Thrane, N. Christensen, and R. Schofield, Phys. Rev. D **87**, 123009 (2013), arXiv:1303.2613 [astro-ph.IM].
- [48] E. Thrane, N. Christensen, R. M. S. Schofield, and A. Effler, Phys. Rev. D **90**, 023013 (2014), arXiv:1406.2367 [astro-ph.IM].
- [49] M. W. Coughlin et al., Class. Quant. Grav. **33**, 224003 (2016), arXiv:1606.01011 [gr-qc].
- [50] Y. Himemoto and A. Taruya, Phys. Rev. D **96**, 022004 (2017), arXiv:1704.07084 [astro-ph.IM].
- [51] M. W. Coughlin et al., Phys. Rev. D **97**, 102007 (2018), arXiv:1802.00885 [gr-qc].
- [52] Y. Himemoto and A. Taruya, Phys. Rev. D **100**, 082001 (2019), arXiv:1908.10635 [astro-ph.IM].
- [53] P. M. Meyers, K. Martinovic, N. Christensen, and M. Sakellariadou, Phys. Rev. D **102**, 102005 (2020), arXiv:2008.00789 [gr-qc].
- [54] K. Janssens, K. Martinovic, N. Christensen, P. M. Meyers, and M. Sakellariadou, Phys. Rev. D **104**, 122006 (2021).
- [55] K. Janssens, G. Boileau, N. Christensen, F. Badaracco, and N. van Remortel, “Impact of correlated seismic and correlated newtonian noise on the einstein telescope,” (2022).
- [56] G. Boileau, N. Christensen, and R. Meyer, arXiv e-prints , arXiv:2204.03867 (2022), arXiv:2204.03867 [gr-qc].
- [57] B. P. Abbott et al. (LIGO Scientific Collaboration and Virgo Collaboration), Phys. Rev. Lett. **120**, 201102 (2018).
- [58] L. Amalberti, N. Bartolo, and A. Ricciardone, Phys. Rev. D **105**, 064033 (2022).
- [59] H. Takeda, A. Nishizawa, K. Nagano, Y. Michimura, K. Komori, M. Ando, and K. Hayama, Phys. Rev. D **100**, 042001 (2019).

Appendix A: Antenna pattern functions for tensorial gravitational waves

We follow the description of the ET’s triangle of the Fig. 1 from [17] but interferometer indices 1,2,3 become X,Y,Z.

We introduce the orthogonal triad in the transverse trace less form as $(\mathbf{e}_x, \mathbf{e}_y, \mathbf{e}_z)$, which allows us to write the basis polarization tensors :

$$\begin{aligned} \mathbf{e}_+ &= \mathbf{e}_x \otimes \mathbf{e}_x - \mathbf{e}_y \otimes \mathbf{e}_y \\ \mathbf{e}_\times &= \mathbf{e}_x \otimes \mathbf{e}_y + \mathbf{e}_y \otimes \mathbf{e}_x \end{aligned} \quad (\text{A1})$$

with $\mathbf{h} = h_+ \mathbf{e}_+ + h_\times \mathbf{e}_\times$ and h_+, h_\times the tensor plus-, respectively cross-polarization components.

The symmetric trace-free tensors representing the three ET interferometers are given by:

$$\begin{aligned} d^X &= \frac{1}{2} \mathbf{e}_1 \otimes \mathbf{e}_1 - \mathbf{e}_2 \otimes \mathbf{e}_2 \\ d^Y &= \frac{1}{2} \mathbf{e}_2 \otimes \mathbf{e}_2 - \mathbf{e}_3 \otimes \mathbf{e}_3 \\ d^Z &= \frac{1}{2} \mathbf{e}_3 \otimes \mathbf{e}_3 - \mathbf{e}_1 \otimes \mathbf{e}_1 \end{aligned} \quad (\text{A2})$$

with the basis of the three arms of the ET’s configuration given by $\mathbf{e}_1; \mathbf{e}_2; \mathbf{e}_3 = \frac{1}{2}(\sqrt{3}, -1, 0); \frac{1}{2}(\sqrt{3}, 1, 0); (0, 1, 0)$.

For each interferometer ($I = X, Y, Z$), the interferometer response $h^I(f)$ is given by the product between the detector tensor \mathbf{d}^I and the tensor \mathbf{h} :

$$\begin{aligned} h^I(t) &= d_{ij}^I h^{ij} = d_{ij}^I e_+^{ij} h_+ + d_{ij}^I e_\times^{ij} h_\times \\ &= F_+^I h_+ + F_\times^I h_\times \end{aligned} \quad (\text{A3})$$

with F_p^I the antenna pattern function of interferometer I for a GW with polarization p .

According to [17], it is possible to write the unit vector of the basis (xyz) in the radiation frame. We introduce the polarization angle ψ as $\cos \psi = \mathbf{e}_\theta \cdot \mathbf{e}_x$, so, we can write the antenna pattern function as a function of the sky position (θ, ϕ) . For example, the antenna pattern function of the interferometer X is :

$$\begin{aligned}
\langle X(f)X^*(f') \rangle &= \frac{1}{2}\delta(f-f') \left[S_n^X(f) + \frac{3}{10}S_h(f) \right] \\
\langle A(f)A^*(f') \rangle &= \frac{1}{2}\delta(f-f') \left[S_n^A(f) + \frac{9}{20}S_h(f) \right] \\
\langle E(f)E^*(f') \rangle &= \frac{1}{2}\delta(f-f') \left[S_n^E(f) + \frac{9}{20}S_h(f) \right] \\
\langle A(f)E^*(f') \rangle &= \frac{1}{2}\delta(f-f') [S_n^{AE}(f) + 0S_h(f)]
\end{aligned} \tag{A13}$$

Appendix B: Antenna pattern functions for non-GR polarization gravitational waves

The non-GR polarization can also be defined from the orthogonal triad ($\mathbf{e}_x, \mathbf{e}_y, \mathbf{e}_z$) [57]. We define two other kind of polarization, the vector (x, y) and scalar (b, l) modes [58, 59].

$$\begin{aligned}
\mathbf{e}_x &= \mathbf{e}_x \otimes \mathbf{e}_z + \mathbf{e}_z \otimes \mathbf{e}_x \\
\mathbf{e}_y &= \mathbf{e}_y \otimes \mathbf{e}_z + \mathbf{e}_z \otimes \mathbf{e}_y
\end{aligned} \tag{B1}$$

and

$$\begin{aligned}
\mathbf{e}_b &= \mathbf{e}_x \otimes \mathbf{e}_x + \mathbf{e}_y \otimes \mathbf{e}_y \\
\mathbf{e}_l &= \mathbf{e}_z \otimes \mathbf{e}_z
\end{aligned} \tag{B2}$$

For interferometer X , the antenna pattern of the non-GR modes are given by,

- Vector modes:

$$\begin{aligned}
F^x(\theta, \phi, \psi) &= \frac{-\sqrt{3}}{2} \sin \theta [\cos \theta \cos \psi \sin 2\phi + \sin \psi \cos 2\phi] \\
F^y(\theta, \phi, \psi) &= \frac{\sqrt{3}}{2} \sin \theta [\cos \theta \sin \psi \sin 2\phi - \cos \psi \cos 2\phi]
\end{aligned} \tag{B3}$$

- Scalar modes:

$$\begin{aligned}
F^b(\theta, \phi) &= \frac{\sqrt{3}}{4} \sin^2 \theta \sin 2\phi \\
F^l(\theta, \phi) &= \frac{-\sqrt{3}}{4} \sin^2 \theta \sin 2\phi
\end{aligned} \tag{B4}$$

The integration over the sky for differences configuration are :

- Vector modes:

$$\begin{aligned}
\int_{sky} (F_x^X)^2 + (F_y^X)^2 &= \int_{sky} (F_x^Y)^2 + (F_y^Y)^2 \\
&= \int_{sky} (F_x^Z)^2 + (F_y^Z)^2 = \frac{3}{10} \\
\int_{sky} (F_y^X F_y^Y) + (F_x^X F_x^Y) &= \int_{sky} (F_y^X F_y^Z) + (F_x^X F_x^Z) \\
&= \int_{sky} (F_y^Y F_y^Z) + (F_x^Y F_x^Z) = -\frac{3}{20}
\end{aligned} \tag{B5}$$

- Scalar modes:

$$\begin{aligned}
\int_{sky} (F_b^X)^2 + (F_l^X)^2 &= \int_{sky} (F_b^Y)^2 + (F_l^Y)^2 \\
&= \int_{sky} (F_b^Z)^2 + (F_l^Z)^2 = \frac{1}{10} \\
\int_{sky} (F_l^X F_l^Y) + (F_b^X F_b^Y) &= \int_{sky} (F_l^X F_l^Z) + (F_b^X F_b^Z) \\
&= \int_{sky} (F_b^Y F_b^Z) + (F_l^Y F_l^Z) = -\frac{1}{20}
\end{aligned} \tag{B6}$$

We can summarize the contribution from an isotropic SGWB to each channel for the different polarizations:

- Vector modes:

$$\begin{aligned}
\langle X(f)X^*(f') \rangle &= \frac{1}{2}\delta(f-f') \left[S_n^X(f) + \frac{3}{10}S_h(f) \right] \\
\langle A(f)A^*(f') \rangle &= \frac{1}{2}\delta(f-f') \left[S_n^A(f) + \frac{9}{20}S_h(f) \right] \\
\langle E(f)E^*(f') \rangle &= \frac{1}{2}\delta(f-f') \left[S_n^E(f) + \frac{9}{20}S_h(f) \right] \\
\langle A(f)E^*(f') \rangle &= \frac{1}{2}\delta(f-f') [S_n^{AE}(f) + 0S_h(f)]
\end{aligned} \tag{B7}$$

- Scalar modes:

$$\begin{aligned}
\langle X(f)X^*(f') \rangle &= \frac{1}{2}\delta(f-f') \left[S_n^X(f) + \frac{1}{10}S_h(f) \right] \\
\langle A(f)A^*(f') \rangle &= \frac{1}{2}\delta(f-f') \left[S_n^A(f) + \frac{3}{20}S_h(f) \right] \\
\langle E(f)E^*(f') \rangle &= \frac{1}{2}\delta(f-f') \left[S_n^E(f) + \frac{3}{20}S_h(f) \right] \\
\langle A(f)E^*(f') \rangle &= \frac{1}{2}\delta(f-f') [S_n^{AE}(f) + 0S_h(f)]
\end{aligned} \tag{B8}$$